Holocene Atlantic climate variations deduced from carbonate periplatform sediments (leeward margin, Great Bahama Bank)

Sven Roth and John J. G. Reijmer
GEOMAR, Research Center for Marine Geosciences, Kiel, Germany

Received 28 January 2003; revised 23 July 2003; accepted 20 October 2003; published 22 January 2004.

[1] A marine sediment core from the leeward margin of Great Bahama Bank (GBB) was subjected to a multiproxy study. The aragonite dominated core MD992201 comprises the past 7230 years in a decadal time resolution and shows sedimentation rates of up to 13.8 m/kyr. Aragonite mass accumulation rates, age differences between planktonic foraminifera and aragonite sediments, and temperature distribution are used to deduce changes in aragonite production rates and paleocurrent strengths. Aragonite precipitation rates on GBB are controlled by exchange of carbonate ions and CO_2 loss due to temperature-salinity conditions and biological activity, and these are dependent on the current strength. Paleocurrent strengths on GBB show high current velocities during the periods 6000–5100 years BP, 3500–2700 years BP, and 1600–700 years BP; lower current speeds existed during the time intervals 5100–3500 years BP, 2700–1600 years BP, and 700–100 years BP. Bahamian surface currents are directly linked to the North Atlantic atmospheric circulation, and thus periods with high (low) current speeds are proposed to be phases of strong (weak) atmospheric circulation. *INDEX TERMS:* 1620 Global Change: Climate dynamics (3309); 3022 Marine Geology and Geophysics: Marine sediments—processes and transport; 4267 Oceanography: General: Paleoceanography; 4512 Oceanography: Physical: Currents; 9325 Information Related to Geographic Region: Atlantic Ocean; *KEYWORDS:* Holocene climate, Great Bahama Bank, Atlantic circulation

Citation: Roth, S., and J. J. G. Reijmer (2004), Holocene Atlantic climate variations deduced from carbonate periplatform sediments (leeward margin, Great Bahama Bank), *Paleoceanography*, *19*, PA1003, doi:10.1029/2003PA000885.

1. Introduction

[2] The Great Bahama Bank (GBB) is the largest shallow-water carbonate platform of the Bahamian archipelago with an average water depth of less than 10 m slightly deepening to the north [*Boss and Rasmussen*, 1995]. On the eastern, windward side, Andros Island is elevated several meters above sea level and is adjacent to the Tongue of the Ocean, an 1800 m deep basin cutting into GBB and separating Andros from New Providence. Northwest and Northeast Providence Channels bound GBB to the north, and the Florida Straits occurs to the west. The Santaren Channel borders the platform to the southwest and the Old Bahama Channel divides GBB from Cuba (Figure 1). Isolated by these deep channels GBB is a pure carbonate province with no terrigenous input [*Carew et al.*, 1998]. Andros and GBB were subaerially exposed from the end of the last interglacial (MIS 5e; 120000 years BP) up to the onset of Holocene flooding, around 7600 years ago [*Carew and Mylroie*, 1997; *Carew et al.*, 1998]. The main shallow-water carbonate production contributing to the periplatform sediments in core MD992201 is restricted to the platform west of Andros Island. The deposits on the platform top consist of lime mud, ooids, grapestones, and coralgal lithofacies [*Newell and Rigby*, 1957; *Purdy*, 1963a, 1963b; *Enos*, 1974].

[3] An important phenomenon, dominating the Bahamian sedimentary system is the occurrence of "whitings" [e.g., *Neumann and Land*, 1975; *Purdy*, 1963a, 1963b; *Ginsburg*, 1956; *Wilber et al.*, 1990]. Whitings are bright, elliptical white patches in the water that occur on the platform top and at the bank margins. Their white color in comparison to the surrounding water masses is the result of the occurrence of concentrated suspension of needle shaped aragonitic sediment in the water column. Whitings are known to produce great quantities of lime mud on the shallow banks of the Bahamas [*Neumann and Land*, 1975; *Hine et al.*, 1981a; *Boardman et al.*, 1986].

[4] Numerous authors [e.g., *Broecker and Takahashi*, 1966; *Milliman et al.*, 1993; *Morse et al.*, 1984; *Shinn et al.*, 1989] have discussed the genesis of these whiting sediments. From age determination of suspended whiting sediments, it has been concluded that at best 25% of the whiting sediment can be attributed to recent inorganic precipitation. The rest is thought to be resuspended older material. On the basis of this assumption, *Boss and Neumann* [1993] calculated a ^{14}C-age of at least 267 years before present for 75% of the whiting material, which is not directly attributable to active precipitation. Through ^{14}C-activity measurements of the aragonitic whiting material, *Broecker and Takahashi* [1966] and *Broecker et al.* [2000] concluded that aragonitic bottom sediments are stirred up and stay in suspension for long periods within the water column. Numerous approaches have been made to investigate aragonite production and sedimentation patterns on GBB: *Lowenstam and Eppstein* [1957] with stable isotopes; *Thompson et al.* [1997] on the basis of microbial activity; *Shinn et al.* [1989] on physical phenomena and inorganic

0883-8305/04/2003PA000885

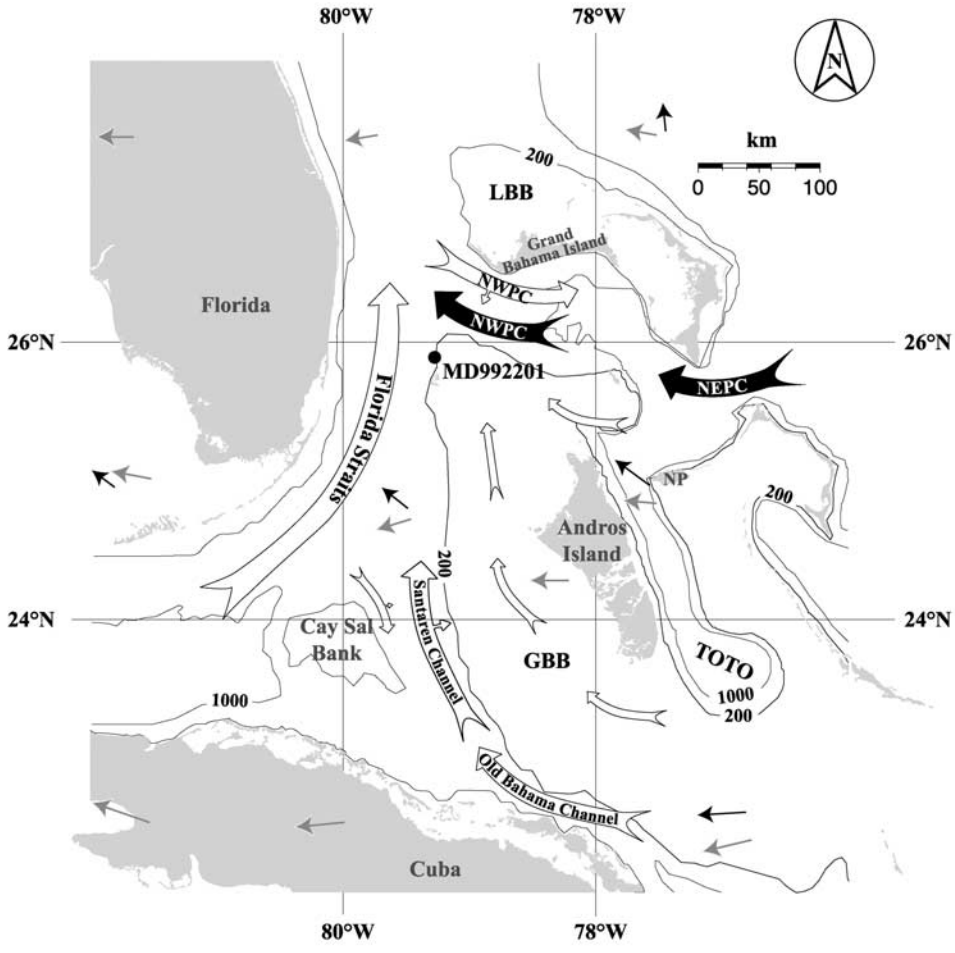

Figure 1. The northern Bahamas with position of core MD992201. Small arrows display the regional wind regime (January, gray; July, black). Open arrows indicate current directions of the upper 50 m surface layer and corresponding cross-stream components [after *Leaman et al.*, 1995]. The platform edges are indicated by the 200 m isobath. NWPC, Northwest Providence Channel; NEPC, Northeast Providence Channel; LBB, Little Bahama Bank; GBB, Great Bahama Bank; TOTO, Tongue of the Ocean; NP, New Providence Island. Wind field data derived from the INGRID database (http://ingrid.ldeo.columbia.edu/). Base map constructed with online map creation (http://www.aquarius.geomar.de/omc/make_map.html).

precipitation; *Robbins et al.* [1997] on lime-mud budgets; *Robbins and Blackwelder* [1992] on biologically induced precipitation; *Milliman et al.* [1993] on Sr-calculations; *MacIntyre and Reid* [1992, 1995] on scanning electron microscope studies (SEM), and *Boss and Neumann* [1993] on physical versus chemical processes. Neither the problem of whiting formation, nor the observed age differences could be reconciled unequivocally. However, all authors concluded that either older bottom sediment or an older carbon source had to be involved in whiting formation and aragonite precipitation.

[5] Sediment transport patterns are related to wind-driven surface currents of the North Atlantic Subtropical Gyre and the North Equatorial Current, delivering water to GBB from the southeast (Figure 1). Density cascading linked to passing winter cold fronts, as proposed by *McCave* [1972], *Wilson and Roberts* [1992, 1995] and *Wilber et al.* [1993], may play an additional role in the mechanics of the off-bank sediment transport.

[6] Today, direct precipitation occurs at the margins of the platform, where geochemical conditions are most favorable due to a high level of supersaturation with respect to aragonite and higher water temperatures, in comparison to the surrounding open ocean [*Demicco and Hardie*, 2002]. After initial precipitation, individual aragonite needles may settle on the seafloor or may stay in suspension, depending on the current conditions on the platform. However, during their transport across the platform individual aragonite precipitates may be deposited or resuspended when the current strength decreases and increases, respectively. Whenever these single aragonite needles are in suspension, they can serve as nuclei for further aragonite precipitation if the chemical conditions are suitable.

Table 1. AMS ^{14}C Dates of Core MD992201 Based on *G. Sacculifer*[a]

Core Depth, cm	Lab Identifier	^{14}C Age, Years BP	Calibrated Calendar Age, Years BP	Calendar Year Range ±2σ, Years BP
10	KIA-17931	475 ± 25	−9	−15–140
125	KIA-14587	560 ± 35	240	107–277
400	KIA-17932	1700 ± 25	1260	1220–1291
670	KIA-14588	1925 ± 35	1480	1384–1544
935	KIA-17939	2710 ± 40	2355	2314–2498
1205	KIA-13969	3285 ± 30	3130	3023–3208
1450	KIA-17934	3745 ± 35	3665	3573–3761
1705	KIA-13970	4195 ± 40	4275	4147–4399
2005	KIA-19771	4830 ± 35	5095	4979–5116
2475	KIA-13972	5490 ± 40	5885	5749–5931
2880	KIA-13973	6020 ± 40	6425	6327–6522
3250	KIA-17936	6295 ± 35	6735	6657–6839
3605	KIA-13974	6530 ± 50	7015	6893–7175
3780	KIA-13975	6590 ± 45	7140	6983–7223

[a]Uncertainties (±) of ^{14}C ages are given as 1σ values, calendar year ranges represent 95% probability (2σ. PMC (corrected) is the proportion of modern (1950 AD) carbon (%), corrected with the δ^{13}C value for mass fractionation.

[7] Oxygen isotope derived temperatures from planktonic foraminifera (*G. sacculifer*) and laser-based grain-size analyses can be used to separate the signals of aragonite accumulation and age offsets in terms of aragonite production and transport. The aragonite transport and production conditions on the platform can be separated using aragonite mass accumulation rates (MAR_{ar}), and the age offsets between the aragonite fraction and the foraminifera. The variation in surface current strength, in combination with changes in the amount of eolian transported iron (Fe), will be used to reconstruct climatic conditions, such as wind field parameters including trade wind strength.

[8] The aim of this study is to give an overview on the changing pattern of aragonite precipitation and sedimentation on GBB; this can be linked to climatic variability and fluctuations in ocean circulation. As a mechanism for the formation of aragonitic whiting sediments, we suggest changing climate, affecting atmospheric circulation (e.g., trade winds) and surface ocean circulation, subsequently influencing carbonate precipitation and export conditions off the GBB platform.

2. Regional Atmospheric Circulation and Oceanography

[9] GBB and the northern Bahamas experience a subtropical to temperate climate influenced by the northeast trade winds. Temperatures range from 18.5°C during winter and 28.5°C in summer. The average annual precipitation amounts to ~1355 mm [*Carew and Mylroie*, 1997]. Temperature and precipitation patterns are strongly bound to the seasonal atmospheric circulation: changing positions and strength of the high and low pressure systems, the Intertropical Convergence Zone (ITCZ), the Subtropical Divergence Zone (STDZ), and the associated trade wind belt. During the northern hemisphere (NH) summer, the atmospheric highs and lows are less pronounced over the North Atlantic Ocean and the STDZ and the ITCZ move northward. The trade winds weaken and high precipitation prevails over the northern Bahamas. Average net evaporation (evaporation-precipitation; E-P) amounts to approx 50 cm/year in the NH summer [*Smith*, 1995]. During the boreal winter, the whole atmospheric regime migrates south with the ITCZ shifting to or south of the equator (5°S). The atmospheric high and low pressure systems strengthen, the easterly trade winds are enhanced, and GBB is under the influence of colder and drier air masses. During NH winter, E-P averages around 225–250 cm/year [*Smith*, 1995]. Throughout the year, GBB is influenced by easterly winds (Figure 1).

[10] The strength and direction of the trade winds are, next to tides, waves and storms, the driving forces of the surface water masses delivered to GBB [*Smith*, 1940; *Cloud*, 1962b; *Purdy*, 1963a]. Long-term net flow measurements over GBB showed a very slow current velocity of ~2 cm/s toward the north (002°N; *Smith* [1995]). This is thought to be the outcome of two almost opposing forces, a tide-induced flow toward the east-southeast and a wind- and density-driven northward flow [*Smith*, 1995].

[11] The North Atlantic Subtropical Gyre is the major source of water mass delivered to GBB and comes from the southeast, passing the Old Bahama Channel and Santaren Channel [*Leaman et al.*, 1995; *Atkinson et al.*, 1995] to join the Florida Current. The surface-layer ocean circulation (approximately the upper 50 m) around GBB and local wind directions are shown in Figure 1.

3. Material and Methods

3.1. Coring and Sampling

[12] In July 1999 a 38 m long sediment core (MD992201) was taken from the Holocene sedimentary wedge on the leeward (western) margin of Great Bahamas Bank (long. 79°16.34′W, lat. 25°53.49′N). The core was retrieved from 290 m water depth with the giant piston corer (40 m device) mounted on the French Research Vessel *Marion Dufresne* (Figure 1). The core catcher was damaged hitting the underlying glacial hardground, suggesting that the entire Holocene carbonate wedge was recovered. The core was sampled at 5 cm intervals. All samples were wet sieved through a 63 μm sieve and the suspended fine fraction (<63 μm) was collected in 5-L jars. The coarse fraction (>63 μm) was oven dried at 60°C. To separate the grain-size fractions, the coarse fraction was dry sieved through 250 μm,

Table 2. AMS ^{14}C Dates of Core MD992201 Based on the Bulk Fraction and Calculated ^{14}C Age Offsets Between *G. Sacculifer* and Bulk Sediment[a]

Core Depth, cm	Lab Identifier	Corrected PMC, %	^{14}C Age, Years BP	^{14}C Age Offsets, Years
10	KIA-17937	89.81 ± 0.32	865 ± 30	390 ± 55
100	KIA-16954	85.24 ± 0.25	1285 ± 25	745 ± 70
400	KIA-17938	79.38 ± 0.32	1855 ± 35	155 ± 70
650	KIA-16955	74.33 ± 0.24	2385 ± 25	510 ± 70
935	KIA-17973	69.70 ± 0.32	2900 ± 35	190 ± 75
1205	KIA-16956	64.47 ± 0.22	3525 ± 25	240 ± 55
1580	KIA-17940	58.30 ± 0.29	4335 ± 40	360 ± 80
2005	KIA-16957	53.12 ± 0.21	5080 ± 25	250 ± 65
2235	KIA-17941	50.10 ± 0.30	5550 ± 50	395 ± 90
2805	KIA-17572	46.25 ± 0.20	6195 ± 35	265 ± 75
3250	KIA-17942	44.85 ± 0.28	6440 ± 50	145 ± 85
3605	KIA-17573	44.38 ± 0.17	6525 ± 30	−5 ± 80
3780	KIA-17943	43.70 ± 0.31	6650 ± 55	60 ± 100

[a]Uncertainties (±) are given as 1σ values for ^{14}C ages and according to least squares method for age offsets between *G. sacculifer* and bulk sediment. PMC (corrected) is the proportion of modern (1950 AD) carbon (%), corrected with the δ^{13}C value for mass fractionation.

500 μm, and 1000 μm sieves. For stable isotope and AMS ^{14}C-measurements, planktonic foraminifera *G. sacculifer* were collected from the >250 μm fraction. Subsamples from the fine fraction (<63 μm) were used for X-ray diffraction. Bulk samples were taken for stable isotope measurements and AMS ^{14}C dating.

3.2. Isotopic Composition

[13] To determine δ^{13}C and δ^{18}O of biogenic carbonate, planktonic foraminifera *Globigerinoides sacculifer* (10 specimens) from the grain-size fraction 250–1000 μm were collected. The samples were prepared following the method of *Wachter and Hayes* [1985] and analyzed on a Finnigan Mat 252 mass spectrometer (University of Erlangen, Germany). All values are given as parts per thousand against the V-PDB standard. The reproducibility of the results was ensured by double measurements. The maximum uncertainty amounts to ±0.06 (1σ values).

[14] To obtain isotopic information on the aragonitic component of the sediments bulk sediment was analyzed. The samples were dried at 50°C and measured at the Leibniz Laboratory in Kiel, Germany.

3.3. AMS ^{14}C Dating

[15] Radiocarbon dating of planktonic foraminifera *Globigerinoides sacculifer* (14 samples) and bulk sediment (13 samples) was undertaken to detect age differences between the platform-derived aragonite and the pelagic signal of *G. sacculifer* for the Mid- and Late Holocene. All dating was carried out at Leibniz-Labor (Kiel, Germany) (Tables 1 and 2). Error ranges of ^{14}C results include numerical statistics, stability of the AMS-device and uncertainty of the subtracted zero effect. Conventional ages are defined after *Stuiver and Polach* [1977]. Reservoir-age correction was performed with the CALIB 4.0 program using the marine calibration curve and a reservoir age of 400 years [*Stuiver et al.*, 1998]. The results show an undisturbed stratigraphic succession throughout the entire core. All ages are given in calendar years before 1950 (years BP).

3.4. Carbonate Mineralogy

[16] X-ray diffraction (XRD) was used to study the mineralogy of the sediment fine fraction <63 μm. To obtain satisfactory results, the grain size of the sediment had to be reduced to 5–10 μm, by carefully grinding for five minutes in an agate mortar. The analysis was carried out on a Philips PW 1700 X-ray diffractometer containing a cobalt anode. The peak-area method was deployed to quantify the aragonite content [*Milliman*, 1974]. The aragonite/calcite peak-area ratios were converted into relative weight percentages using an in-house calibration curve. Weight percentages of HMC and LMC were directly calculated by their peak-area ratios.

3.5. Mass Accumulation Rates

[17] Bulk mass accumulation rates (MAR_{bulk}) were calculated using the linear sedimentation rate (LSR) and the dry bulk densities (DBD) of the individual samples after *Ehrmann and Thiede* [1985]:

$$MAR_{bulk}\left(g\ cm^{-2}\ yr^{-1}\right) = LSR\left(cm\ yr^{-1}\right) \bullet DBD\left(g\ cm^{-3}\right).$$

The LSR (cm yr^{-1}) is the length of a specified sediment section (cm) divided by the duration, required for sedimentation (years). The DBD (g cm^{-3}) is defined as the sediment weight of the sample (g) divided by the bulk volume (cm^{-3}) of the sample (sediment volume and pore space volume), with pore-space volume being equivalent to the water content of the individual samples. Proportions of the MAR_{bulk} for the different sediment components are calculated by multiplication of the MAR_{bulk} with the percent amount of individual mineralogic components, obtained through XRD (e.g., aragonite, HMC, LMC):

$$MAR_{ar}\left(g\ cm^{-2}yr^{-1}\right) = MAR_{bulk}\left(g\ cm^{-2}yr^{-1}\right) \bullet \%aragonite \bullet 100^{-1}$$

3.6. Laser Grain-Size Analysis and SEM Images

[18] A detailed study of grain sizes was performed on the 0.16 μm–600 μm fraction of bulk sediment. The deployed instrument Analysette 22 Laser Particle Sizer (Fritsch

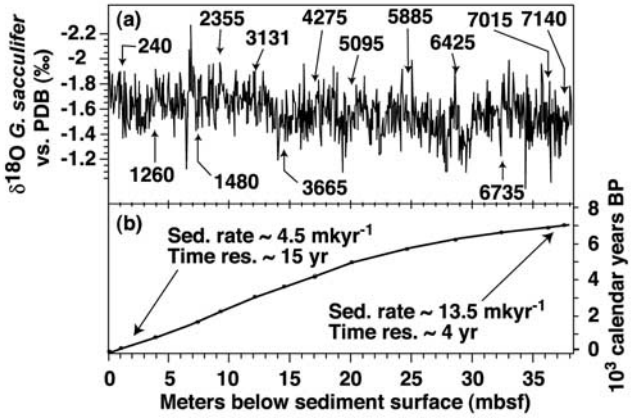

Figure 2. (a) $\delta^{18}O$ data from foraminifera (*G. sacculifer*) for sediment core MD992201 and radiocarbon dates marked by arrows. (b) Linear sedimentation rates. All ages are given in calendar years before 1950 (years BP).

Instruments, Germany) measures the grain sizes via laser diffraction using a combination of Fraunhofer and full Mie scattering theory. SEM analyses of the bulk sediment were made at the University of Kiel (Germany) with a CamScan Cs 44 (PA, U.S.A) to investigate the nature of the aragonitic sediments.

3.7. Relative Current and Aragonite Productivity Index

[19] Mass accumulation rates of aragonite (MAR_{ar}) and age differences between the aragonite fraction and the foraminiferal ages have been used to quantify relative changes in current strength and aragonite productivity. Laser diffraction based grain-size analysis was used to confirm the deduced current strengths. Current strength was qualitatively classified into five categories depending on changes in the aforementioned parameters: very high (v.h.), high (h.), moderate (m.), low (l.), and very low (v.l.). For aragonite productivity, a classification into high (h.), moderate (m.), and low (l.) production rate was made. Deduced current speeds and aragonite production potential were interpreted in terms of paleoclimate and paleoceanography.

4. Results

4.1. Foraminiferal Ages

[20] The chronology of core MD992201 is based on 14 AMS ^{14}C-dates on planktonic foraminifera *G. sacculifer* (Figure 2). The ^{14}C-ages, PMC (percent modern carbon), calibrated calendar years, are given in Table 1. Through linear extrapolation, a core-top age of −20 years BP was determined. The core base was dated to 7230 years BP. With the sampling interval of 5 cm a decadal time resolution in the upper part and a bidecadal resolution in the lower part of the core could be obtained (Figure 2). No gravity flows or erosional features were observed, pointing to a continuous record of deposition from suspension and traction currents for the last 7230 years.

4.2. Aragonite Ages

[21] The aragonitic sediments were produced on the platform top and subsequently exported to the core site. To obtain the age of the aragonite from the platform, 13 AMS ^{14}C-dates were obtained from the bulk sediments (Table 2). Differences between the ages from the foraminifera and the aragonite-dominated sediments range from 0 years at the base of the core to 770 years at 215 years BP (Figure 3). From the core bottom (7230 years BP) to ~5565 years BP, the age difference increases from 0 to about 395 years, followed by a decrease to 250 years at 5200 years BP. The time interval from 5200 to 4430 years BP is characterized by an increase in the age offset to a value of 360 years prevailing at this level until 4065 years BP. A gradual decline in age offset from 370 to 190 years marks the time slice from 4065 to 2395 years BP followed by a steep increase to age offsets of about 510 years (2395–1460 years BP). A sharp drop to a 155-year age difference from 1460–845 years BP precedes the most drastic rise in age offsets starting at 845 years BP and reaching maximum values of about 775 years at 215 years BP. The youngest time interval (215 years BP-recent) is characterized by declining age offsets between foraminifera and aragonite. The uppermost date was obtained from a depth of 10 cm in the core (−10 years BP) and shows an age difference of 390 years. Extrapolated core-top values would result in age offsets of about 370 years.

4.3. Carbonate Mineralogy

[22] Bulk carbonate content varies from 86–97 weight percent (wt %). Aragonite dominates with 97 wt % in the lower part of the core, decreasing gradually to 88 wt % toward the top of the core (Figure 4). High magnesium calcite (HMC), mainly produced on the platform by red algae is the second major carbonate phase and varies between 1.5–10 wt %, with increasing values up through the core. The pelagic signal is represented by low magnesium calcite (LMC), which makes up 0.5–3 wt % of the bulk sediment.

4.4. Mass Accumulation Rates (MAR)

[23] Aragonite accumulation dominates the sedimentary system of GBB. The Overall accumulation ratio of the

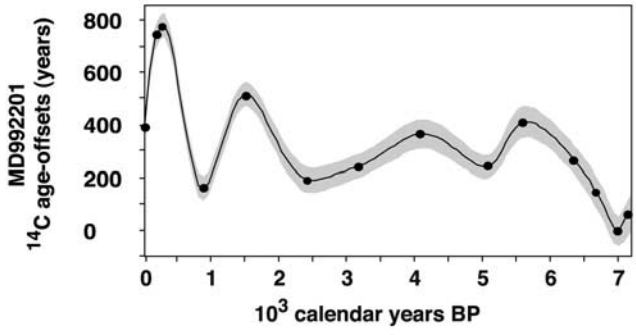

Figure 3. Offsets between ages from foraminifera and aragonite. Error range includes numerical statistics, stability of the AMS-device and uncertainties of the subtracted zero effect.

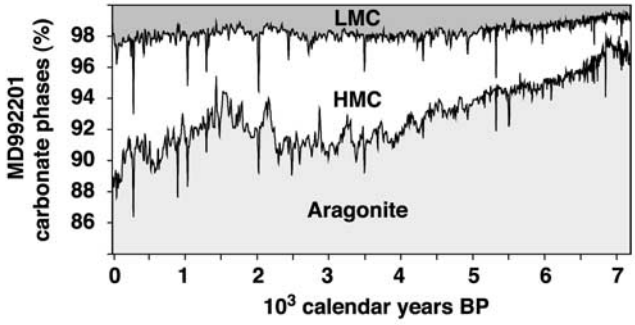

Figure 4. Carbonate mineralogy of core MD992201. LMC, low-magnesium calcite; HMC, high-magnesium calcite.

individual carbonate phases is approximately Ar:HMC:LMC = 100:10:1. The MARs show that the percent HMC increase up-core, observed by XRD (Figure 4), is an effect of negative aragonite dilution and therefore of decreasing aragonite input up-core (Figure 5). The MAR_{HMC} chart behaves similar to the MAR_{LMC} graph and fluctuates on a millennial timescale. However, as the MAR_{HMC} record is not relevant for this study, it will not be addressed further.

4.5. Aragonite Mass Accumulation Rates (MAR_{ar})

[24] GBB was subaerially exposed from the end of the last interglacial (MIS 5e) up to the renewed flooding in the Holocene [*Carew and Mylroie*, 1997; *Carew et al.*, 1998], which commenced approximately 7600 years ago [*Boss and Rassmussen*, 1995; *Fairbanks*, 1989].

[25] Approximately 7230 years BP, aragonite accumulation started abruptly with values of 1.8 $gcm^{-2}yr^{-1}$, decreasing to 0.9 $gcm^{-2}yr^{-1}$ within the first decades (Figure 5). The time interval from 7150–6750 years BP is marked by a strong increase of MAR_{ar} from 0.9 to 1.7 $gcm^{-2}yr^{-1}$, followed by a decrease (6750–5800 years BP) to 0.4 $gcm^{-2}yr^{-1}$. Another sharp drop in MAR_{ar} is visible from 5600 to 5200 years BP followed by a gradual decline, reaching its minimum at 4600 years BP (0.2 $gcm^{-2}yr^{-1}$). A stepwise increase marks the time slice from 4600 to 3100 years BP reaching values as high as 0.65 $gcm^{-2}yr^{-1}$. This interval of high aragonite accumulation is terminated by a sharp decrease of MAR_{ar} (to 0.2 $gcm^{-2}yr^{-1}$) within 200 years, followed by a slight stepwise decrease from 0.2 to 0.18 $gcm^{-2}yr^{-1}$ (2900–1850 years BP). The next period of elevated aragonite accumulation (1550–700 years BP; 0.6 $gcm^{-2}yr^{-1}$) was preceded by a strong increase of MAR_{ar} from 1850 to 1550 years BP. The Little Ice Age (LIA; 700–155 years BP) is characterized by low MAR_{ar} (around 0.3 $gcm^{-2}yr^{-1}$). From 155 years BP to today MAR_{ar} increases to values of ~0.5 $gcm^{-2}yr^{-1}$.

[26] Within the first 2630 years of aragonite accumulation, (7230–4600 years BP) gradients of change were very steep. The long-term trend from the beginning of aragonite accumulation to 4600 years BP shows a gradual decline of MAR_{ar} from 1.8 down to 0.2 $gcm^{-2}yr^{-1}$. The Younger Holocene succession (4600 years BP-recent) shows MAR_{ar} fluctuating around ca. 0.4 $gcm^{-2}yr^{-1}$. Intervals of elevated and decreased MAR_{ar} fluctuate on a millennium timescale (550–1500 years).

4.6. LMC Mass Accumulation Rates (MAR_{LMC})

[27] MAR_{LMC} values are generally low compared to MAR_{ar} throughout the entire core ranging from 0.002 to 0.2 $gcm^{-2}yr^{-1}$ (Figure 5). LMC accumulation starts at 7230 years BP with low values of 0.008 $gcm^{-2}yr^{-1}$ prevailing for about 430 years until 6800 years BP. The following 50 years are characterized by a steep increase up to values of 0.017 $gcm^{-2}yr^{-1}$ (6800–6750 years BP). The time interval from 6750–6300 years BP is characterized by high MAR_{LMC} of 0.017–0.018 $gcm^{-2}yr^{-1}$. A sharp drop in MAR_{LMC} occurs from 6300 to 6275 years BP, to values of 0.007 $gcm^{-2}yr^{-1}$. These conditions prevail to 5750 years BP followed by a sharp increase of MAR_{LMC} to values of 0.02 $gcm^{-2}yr^{-1}$. From 5600 to 4600 years BP MAR_{LMC} shows a gradual decline to 4600 years BP with values around 0.005 $gcm^{-2}yr^{-1}$. This low is followed by a phase (4600–3100 years BP) of high MAR_{LMC} (0.014 $gcm^{-2}yr^{-1}$). This interval of high LMC accumulation is terminated by a sharp decrease of MAR_{LMC} (to 0.006 $gcm^{-2}yr^{-1}$; 3100–2900 years BP). From 2900 to 1550 years BP values gradually decline to 0.003 $gcm^{-2}yr^{-1}$. These low MAR_{LMC} values are followed by a sharp increase to 0.012 $gcm^{-2}yr^{-1}$ within four decades (1550–1510 years BP). These high accumulation rates prevail for about 900 years until 700 years BP, the onset of the LIA. The LIA is characterized by overall low LMC accumulation rates around 0.006 $gcm^{-2}yr^{-1}$ showing two minima (550–450 years BP, around 200 years BP) interrupted by one maximum (340–300 years BP). In

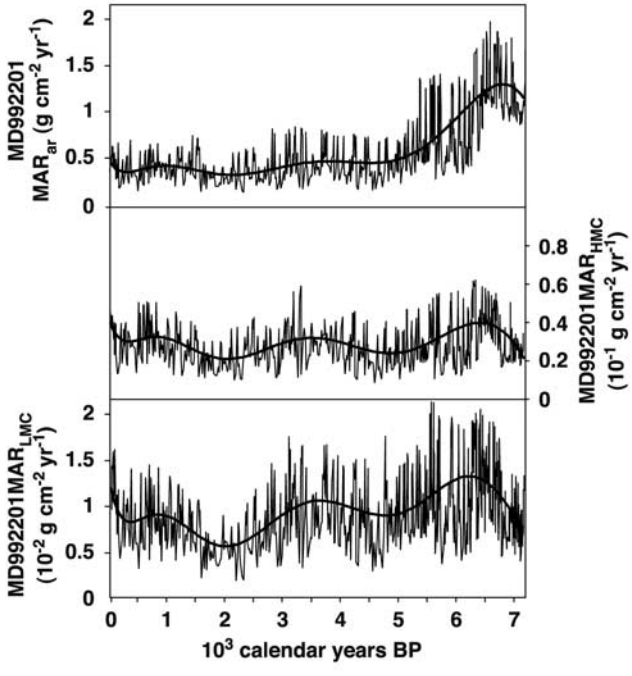

Figure 5. Mass accumulation rates of aragonite (MAR_{ar}), high-magnesium calcite (MAR_{HMC}), and low-magnesium calcite (MAR_{LMC}); polynomial fit, thick lines. Note dimension ratios: ar:HMC:LMC = 100:10:1.

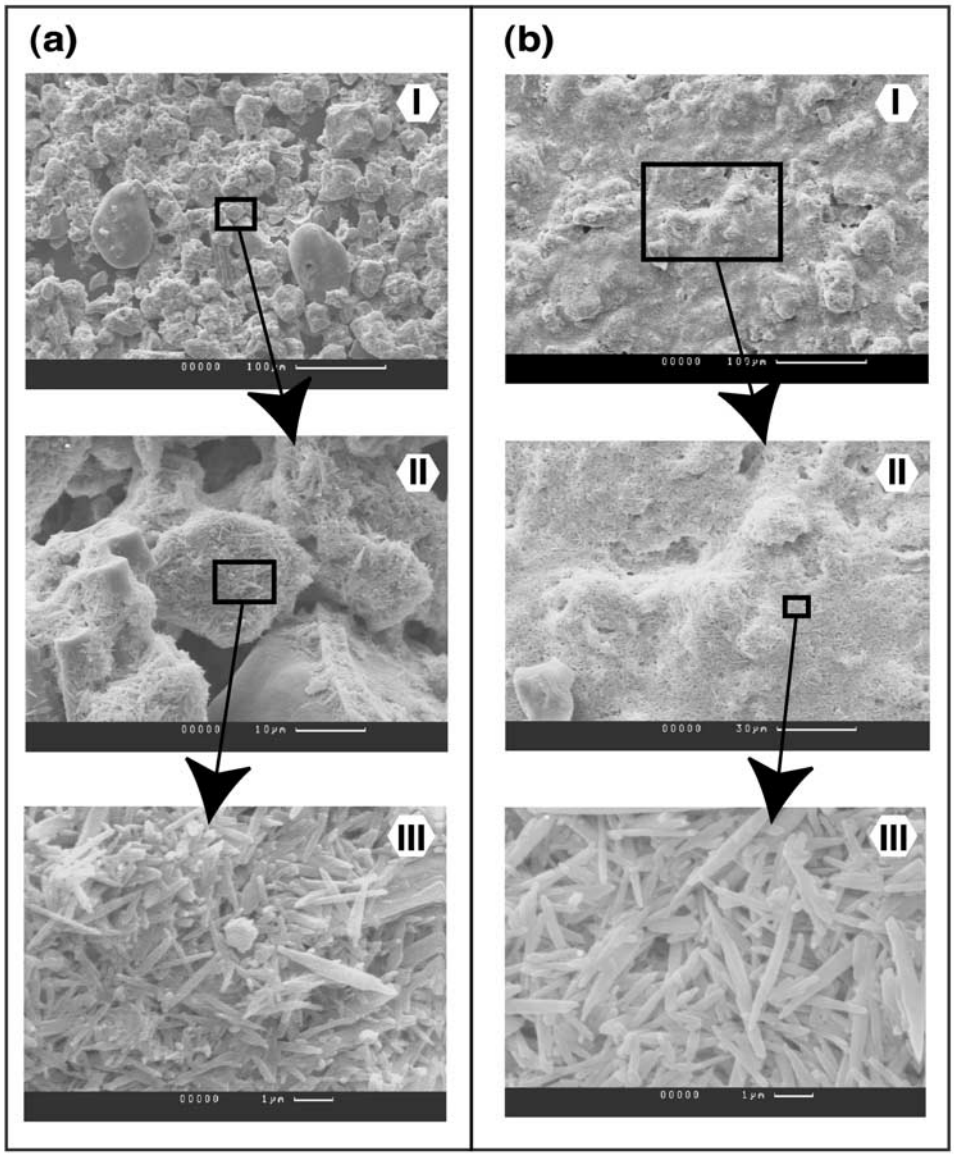

Figure 6. SEM photographs of core MD992201. Magnification is 250x (I), 2000x (II), and 10000x (III), respectively. (a) Images at 1 m core depth corresponding to 185 years BP and (b) at 33.5 m core depth corresponding to 6810 years BP. The difference between samples, consisting predominantly of spherolitic structures, 35–80 μm sized (Figure 6a) and samples with dominating single aragonite needles, 1–5 μm in size (Figure 6b) is clearly illustrated. The elongated, bladed, and pointed shape of the individual crystals with poorly developed crystal faces is well recognizable in both samples.

contrast to the MAR_{ar}, LMC accumulation rates do not show any long-term trends throughout the entire sediment core. Values range around 0.01 $gcm^{-2}yr^{-1}$ throughout the complete succession (Figure 5). Times of elevated and reduced MAR_{LMC} fluctuate on a millennium timescale (1500–2500 years).

4.7. Laser Grain Sizes and SEM

[28] The sediments of MD992201 are uniform throughout the entire core. The fine fraction (<63 μm) makes up 35–98 wt % of the sediments. As the measurements via laser diffraction assume perfect, spherical grains [*Loizeau et al.*, 1994; *Agrawal et al.*, 1991; *Singer et al.*, 1988], which is not the case for the sediments of MD992201 the results can only be interpreted with a detailed knowledge of the sediments provided by SEM images. These show that aragonite occurs in two forms: single 1–5 μm long, needle-shaped, bladed, mostly pointed precipitates and 35–80 μm angular aggregates of single needles (Figure 6). The transition from preferentially single needles to aggregate formation occurs at approximately 6000 years BP. The mechanism for aggregate formation is unknown. It is assumed that all aragonite (single or aggregated needles) was precipitated on the platform top and then transported to the core site by currents coming off the platform [*Wilson and Roberts*, 1992, 1995; *Hine et al.*, 1981a, 1981b]. The bladed, single needles

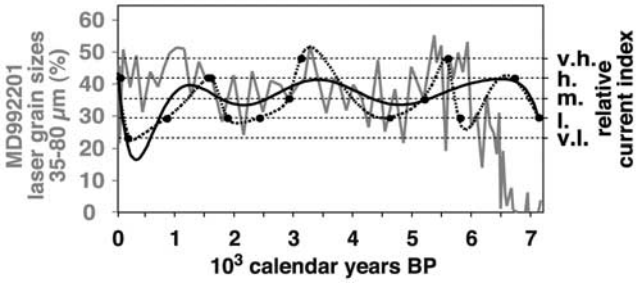

Figure 7. Laser grain size analyzed aragonite cluster abundance (gray line). Note that the laser grain sizes for the first ~1500 years (7200–6000 years BP) are not representing current conditions, but the transition from occurring single aragonite needles to preferred aggregate formation. Deduced relative current strength (black dots), interpolation of points (broken thick line), and polynomial fit (thick black line) are shown. Relative current speed classification: v.h., very high; h., high; m., moderate; l., low; v.l., very low (overview of index markers in Table 3).

would require less strong currents than the much larger aggregates. Therefore intervals of elevated aggregate abundance in the sediments of the core can be interpreted as phases of increased current strength over the GBB platform. No aragonitic marine cements were observed (Figure 6).

[29] To obtain information about the relative abundances of the aggregates in the sediment, grains within the classes from 35 to 80 μm were added up and converted into relative percentages (Figure 7). After the onset of sedimentation at 7230 to 6700 years BP, aggregate abundances are very low, 0 to 3%, followed by a two-step increase to 35% at 5900 years BP. High values (40–55%) until 5100 years BP suggest relatively strong surface currents. Lower current speeds occurred during 5100–3800 years BP, with lowest values (<25%) from 4900 to 4500 years BP. During 3800–2600 years BP surface currents were stronger, as indicated by aggregate percentages up to 52%, followed by lower abundances around 30–40% at 2600–1100 years BP. The Medieval Warm Period (MWP) is characterized by overall elevated aggregate abundance up to 50–52% around 1100–850 years BP. Aggregate abundances and current speeds drop at the onset of the LIA (~650–155 years BP) and remain relatively low until ~150 years BP, when aggregate abundances increase again, showing an upward trend until recent times. Phases of high and low aggregate abundance alternate in a 2000 to 2500-year mode (Figure 7).

5. Discussion

[30] During the discussion on the genesis of whitings and the Bahamian aragonites, it was noted that the suspended aragonitic material and the aragonites on the seafloor were ~200 years older than the surrounding water body [e.g., *Broecker and Takahashi*, 1966; *Milliman et al.*, 1993; *Morse et al.*, 1984; *Shinn et al.*, 1989; *Boss and Neumann*, 1993]. These authors investigated water samples (within and outside the whitings) and sediment surfaces on the platform itself and thus their ages relate to the situation at the present time. We have been able to investigate the age discrepancies further and therefore environmental conditions on GBB throughout the Middle and Late Holocene.

[31] Aragonite production on GBB is dependent on water depth, distance from the platform margin and residence times of the water masses on the platform [e.g., *Demicco and Hardie*, 2002; *Broecker and Takahashi*, 1966]. These parameters, as well as current-dependent residence times, have an impact on the aragonite saturation state of the platform waters, which is of major importance for aragonite precipitation [*Morse and Mackenzie*, 1990; *Morse and He*, 1993; *Langdon et al.*, 2000]. The CO_2 solubility in seawater decreases with increasing temperature and to a lesser extent with increasing salinity [*Morse and He*, 1993; *Duan and Sun*, 2003]. Decreased ΣCO_2 (H_2CO_3, HCO^{3-}, CO_3^{2-}) raises the aragonite saturation and promotes precipitation [*Morse and He*, 1993]. As a result of carbonate precipitation, $CaCO_3$ is lost from the water column and this decreases the saturation state of the GBB platform waters with respect to aragonite with increasing residence times [*Broecker and Takahashi*, 1966; *Broecker et al.*, 2000].

Table 3. Overview of Discussed Evolution of MAR_{ar} and Age Offsets and Resulting Deduced Relative Current Strength and Aragonite Production Patterns[a]

Time Interval, Years BP	Marker Position, Years BP	Dynamics of MAR_{ar}	Age Offset, Years	Relative Current Index	Aragonite Production Index
7230–7150	7150	slight decline	± none	l.	l.
7150–6735	6735	increase	± 0 to 145	h.	h.
6735–5800	5800	strong decrease	145 to 350	l.	l.
5800–5600	5600	increase	350 to390	v.h.	l.
5600–5200	5200	sharp decrease	390 to 250	m.	h.
5200–4600	4600	gradual decrease	250 to 310	l.	l.
4600–3100	3100	stepwise increase	310 to 235	v.h.	m.
3100–2900	2900	marked drop	235 to 220	m.	m.
2900–2400	2400	stepwise decrease	220 to 190	l.	h.
2400–1850	1850	decrease	190 to 375	l.	m.
1850–1600	1600	slight increase	375 to 465	h.	l.
1600–1550	1550	sharp increase	465 to 470	h.	m.
1550–820	820	increase	470 to 175	l.	m.
820–155	155	decrease	175 to 760	v.l.	l.
155 to −20	core top	increase	760 to 390	h.	m.

[a]Dynamics leading to the classification of indices are described in text. Indices are as follows: v.h., very high; h., high; m., moderate; l., low; v.l., very low. Note inverse sorting of ages according to description in text.

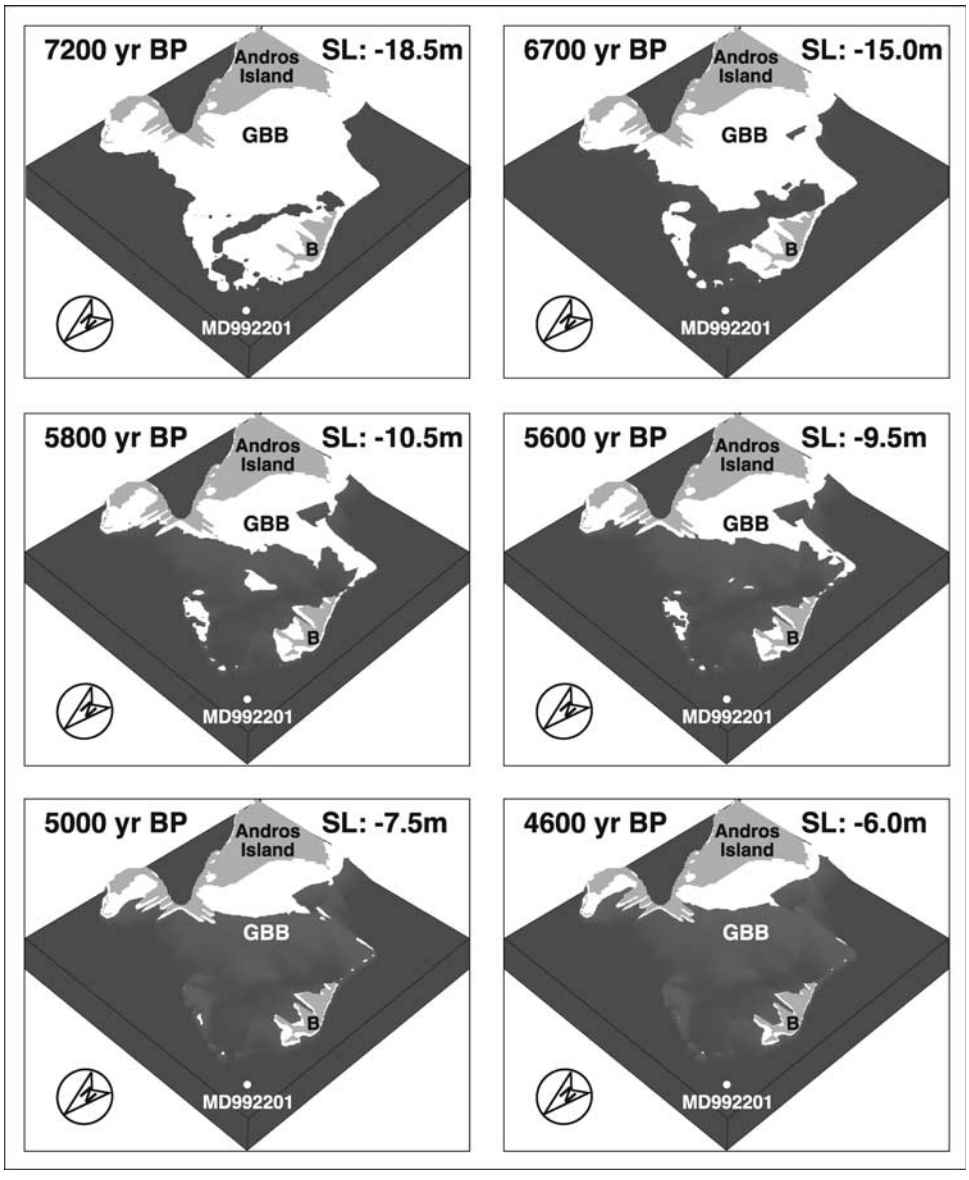

Figure 8. Snapshots of Holocene sea-level rise viewed from the northwest. GBB, Great Bahama Bank; B, Bimini Island; white dot, MD992201 core site. Subaerially exposed platform is indicated by light (yellow) color, flooded platform area is light gray (light blue), and the surrounding water mass is dark gray (dark blue). Paleobathymetry from S. K. Boss (personal communication, 2002); sea-level curve from *Fairbanks* [1989]. See color version of this figure in the HTML.

Thus, next to climatic conditions (insolation, temperature), current-induced water exchange on the platform is the key agent for aragonite production potential.

[32] The aragonitic sediments, which accumulated in the region of the core site were produced on the platform and are subsequently transported off-bank. Today the net flow of water over GBB toward the north amounts to ~2 cm/s [*Smith*, 1995]. Therefore aragonite accumulation rates (MAR_{ar}) at the core position, as well as the age offsets (between aragonitic sediments and planktonic foraminifera), are a combination of aragonite production (active precipitation) and current-induced transport conditions.

[33] The changes in surface current strength (Figure 7) can be deviated by combining the aragonite accumulation rates and the varying aragonite ages. The laser-based grain-size analysis supports the deduced current strength parameters. The evolution and dynamics of index classifications are discussed in the text and reported in Table 3.

[34] Sediment accumulation at the core site started at 7230 years BP with the onset of platform flooding. Flooding of GBB and aragonite production started in the deeper northwestern area of GBB (based on the paleobathymetry of *Boss and Rasmussen* [1995] and S. K. Boss, personal communication, 2002). At this time, no offset exists in the ages from foraminifera and aragonite, suggesting direct off-bank transport of the platform precipitates without any residence of the aragonite on the bank. The rise in aragonite accumulation within the first ~500 years (7200–6700 years

BP) could have resulted from the bathymetric structure of the deeper northwestern platform, with the continuing rise in sea level enlarging the platform production area (Figure 8). During this time interval, age differences rise from initially zero to approximately 145 years, pointing to a successive input and admixture with earlier precipitated aragonites. As the northern platform was still not completely flooded, and thus not overflown by northwesterly currents (open water ways existed only to the north; Figure 8), an increase in the transport distance to the core site most likely explains the observed increase in age offset. An important factor for aragonite precipitation is the CO_2-removal from the water column, which can be achieved through heating (de-gassing) or photosynthetic activity, increasing the degree of super-saturation with respect to aragonite. With the same energy provided by insolation, shallower areas of the platform would become more intensely heated than the deeper regions. The main location of aragonite production may have shifted successively with increasing sea-level rise and platform flooding to the shallower, more southern part of the northern platform, thus increasing the transport distance to the area of the core (Figure 8). Strongly decreasing MAR_{ar} and increasing age differences (145 to 360 years) characterize the time interval from 6700 to 5800 years BP. The amount of aragonitic sediments delivered to the site of the core decreased and the age offsets increased, indicating a lower new aragonite production rate and a further increase of the transport distance (Figure 8). During the period 5800–5600 years BP, increasing MAR_{ar} occurs with an increase in age difference from 350 to 390 years. This suggests a situation of stable or slightly lowered new aragonite production rate, balanced by a strong increase in off-bank transport, probably related to the first occurrence of open-water connections to the southwest (Figure 8). The following 400 years (5600–5200 years BP) are characterized by another sharp drop in aragonite accumulation, whereas the aragonite age offsets decrease from 390 to 250 years. In this time slice, decreasing off-bank transport leads to a drop in MAR_{ar} while the decreasing age offset indicates enhanced new aragonite production. A gradual decrease in MAR_{ar} and increasing age offsets (250 to 310 years) mark the time interval from 5200 to 4600 years BP. In addition to the decreasing transport values, new production of aragonite ceases, resulting in a decrease in aragonite accumulation rates and an increase of age offsets.

[35] During the complete time interval from 7230 to 4600 years BP sea level was steadily rising, and between 5000 and 4600 years BP the platform became entirely overflown by the surface currents from the south-southeast (Figure 8). Gradients of accumulation-rate change were very high. During the phase of initial platform flooding (7230–5600 years BP; $MAR_{ar} > 1.1$ gcm^{-2}yr^{-1}) most of the platform would have been exposed to meteoric subaerial dissolution, which would have resulted in a high amount of carbonate ions, elevating the level of supersaturation in the already flooded areas. Moreover, strong temperature elevation and intense evaporation must have existed in the initially flooded semi-opened basin, promoting aragonite precipitation (Figure 8). At the time the platform was entirely flooded, erosion on the platform stopped, open-marine conditions prevailed and the platform was completely overflown by currents from the southeast. These new conditions on the platform top stopped the steep declining long-term trend (up-core) of aragonite accumulation. Changing temperature on the platform top due to decreasing net insolation may well have had a large impact on production conditions. However, there is no way to quantify these effects. Accumulation rates and their gradients of change from 4600 years BP until today are lower than those of the preceding 2630 years, with values fluctuating around 0.4 gcm^{-2}yr^{-1}.

[36] Between 4600 to 3100 years BP, MAR_{ar} shows a stepwise increase with decreasing age offsets (310–235 years). This suggests renewed aragonite production and an increase in current strength. The latter must have decreased drastically during the time slice of 3100 to 2900 years BP, when MAR_{ar} dropped markedly, since age discrepancies (235–220 years) remain unaltered, indicating no change in new production rates. Slightly better conditions for new production account for the decrease in age differences (220–190 years) during the interval from 2900 to 2400 years BP. The stepwise decrease in MAR_{ar} results from an ongoing decrease in current strength. Low surface current velocities and a strong decrease in new production are suggested by a decrease in MAR_{ar} and an increase in age offsets (190–375 years) during 2400 to 1850 years BP. Surface currents must have increased from 1850–1600 years BP as the MAR_{ar} increases slightly. Rising age offsets (375–465 years) point to a continued decrease in new aragonite production. A sharp increase in MAR_{ar} within 50 years (1600 to 1550 years BP) marks the onset of the medieval warm period (MWP). During the MWP (1550 to 820 years BP) MAR_{ar} increased, whereas age offsets decreased markedly (470–175 years). A higher new production rate and prevailing strong currents are proposed for this time interval. The most drastic increase of age differences for the entire core (175 to 760 years with a maximum of 775 years at 240 years BP) is found between 820 to 155 years BP (LIA). In this time interval, strongly depressed temperatures accompany low MAR_{ar}. A very low new production and distinctly weaker current strength must have existed during this time span. The uppermost core section (155 years BP-recent) is characterized by increasing MAR_{ar}, and decreasing age offsets (760–370 years), which points to a recovering of the new aragonite production rate and increasing current strength.

[37] Combining the aragonite accumulation rates and the varying aragonite ages allows the reconstruction of relative intensities and changes in surface current strength. The laser-based grain-size analysis supports the deduced current strength parameters (Figure 7).

5.1. Impact of Storms and Hurricanes

[38] Major impacts of storms and hurricanes have been described from various locations around the Bahamas [e.g., *Neumann and Land*, 1975; *Hine and Neumann*, 1977; *Hine et al.*, 1981a, 1981b]. With respect to storm frequency and intensity, periods of enhanced storminess are a matter of changing atmospheric conditions, like changes in trade

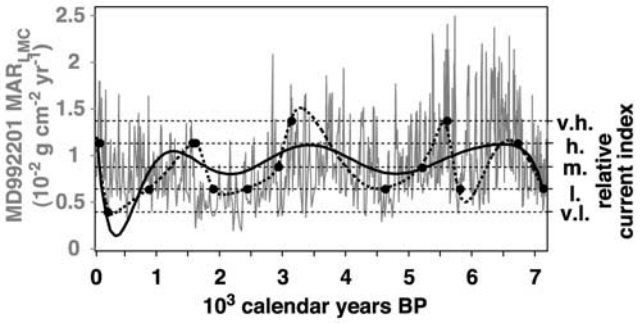

Figure 9. MAR_{LMC} (thin gray line); deduced relative current strength (black dots); interpolation of markers (broken black line); and polynomial fit (thick black line). Relative current speed classification: v.h., very high; h., high; m., moderate; l., low; v.l., very low (overview of index markers in Table 3).

wind strengths and westerlies, operating on seasonal and annual to decadal/interdecadal timescales, comparable to today's NAO positive versus NAO negative conditions, which unequivocally are atmospherically steered, or on even longer timescales. Interannual variations and single events are not detectable in core MD, whereas interdecadal to decadal changes are recorded. For this study, thus single events like hurricanes and storms do not play a major role, while the continuous surface-current system on GBB is driven by atmospheric conditions. Moreover, no storm or hurricane events were detectable in the sedimentary record of the well-dated core MD992201. However, it cannot be ruled out that depending on the track and direction, major storms and hurricanes contributed to sediment input elsewhere at the Holocene sedimentary wedge around GBB, as proposed by *Neumann and Land* [1975], *Hine and Neumann* [1977] and *Hine et al.* [1981a].

5.2. Current Strengths and Atmospheric Circulation

[39] According to our data, current strength was relatively high during 6000–5100 years BP, 3500–2700 years BP, and 1600–700 years BP, whereas the time intervals 5100–3500 years BP, 2700–1600 years BP, and 700–100 years BP are characterized by relatively low current strengths (Figure 7). These findings are in agreement with *Mulder et al.* [2002], *Heilemann* [2000], and *Sierro et al.* [1999], who postulated an increase of current strength around 4000–3000 years BP in the Gulf of Cadiz, which was linked to the thermohaline circulation (THC) in the current pattern. As the dominant, if not total proportion of the surface water masses reaching and flowing over GBB is of North Atlantic origin [*Wajsowicz*, 2002; *Lee et al.*, 1996], the deduced current strengths are suggested to be a direct measure of the North Atlantic Subtropical Gyre, which in turn is strongly dependent on the location and the strength of the North Atlantic atmospheric circulation (northeasterly trades and westerlies). Therefore surface current strength on GBB is directly linked to the strength and location of the trade wind system and oceanographic circulation.

[40] Time intervals with strong surface currents represent phases of strong northeasterly trade winds and strong westerlies with the Intertropical Convergence Zone (ITCZ) being depressed at or south of the equator. As a result of the stronger wind system there would have been increased eolian input of Saharan dust into the low latitude North Atlantic [*Moulin et al.*, 1997; *Sarnthein et al.*, 1981]. Iron (Fe) is known as a major limiting factor for productivity in oligotrophic ocean areas. Recent seasonal variations of eolian dust input have been shown to correlate positively with chlorophyll concentrations in the tropical and subtropical Atlantic [*Hernandez et al.*, 2001]. Moreover, increased wind-induced upwelling would enhance productivity in the Caribbean [*Nyberg et al.*, 2002]. Phases of strong surface currents (and therefore high trade wind speeds) correlate with times of elevated MAR_{LMC}, made up mainly by planktonic foraminifera and coccolithophorids (Figure 9).

[41] An Al/Ti ratio of 15.6 and a Fe/Al ratio of 0.84 characterize average continental crust [*Murray and Leinen*, 1996; *Taylor and McLennan*, 1985]. The terrigenous origin of the eolian transported fraction in the sediments of core MD992201 is illustrated by their Fe/Al- (average 0.55) and Al/Ti-ratios (average 14.6). Figure 9 illustrates the close relationship of planktonic foraminiferal abundances and Fe accumulation in the studied sediment core. Both, increased upwelling and elevated eolian Fe input enhance productivity. Therefore planktonic foraminiferal abundances and MAR_{LMC} are enhanced during periods of strong surface currents (and enhanced atmospheric circulation).

[42] During phases of weak surface currents (low trade wind speeds) with the ITCZ being farther north, upwelling rates would decrease and the eolian Fe transport (Saharan dust) would cease. Consequently, productivity is lower during these time intervals (Figures 9 and 10).

5.3. Aragonite Productivity

[43] Oxygen isotope derived temperatures from the planktonic foraminifer *G. sacculifer* and the deduced aragonite production potential show a strong correlation (Figure 11). This supports the findings of *Morse and He* [1993],

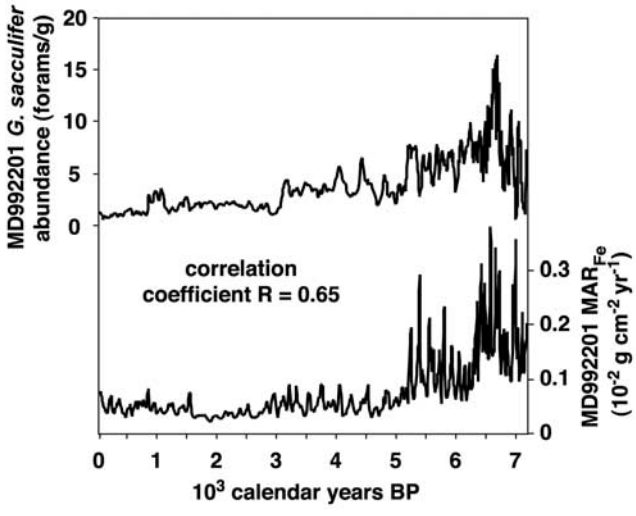

Figure 10. Planktonic foraminiferal abundances (*G. sacculifer*/*G. ruber*) versus eolian Fe input (5-point running means).

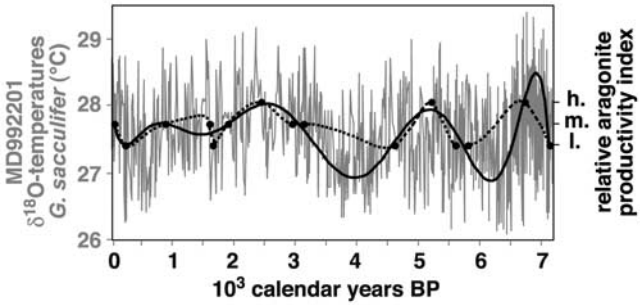

Figure 11. $\delta^{18}O$ (*G. sacculifer*) derived temperatures (thin gray line) versus relative aragonite production potential (markers, black dots); interpolation of markers (broken black line); and polynomial fit (thick black line). Classification of relative aragonite productivity markers: h., high, m., moderate; l., low. Classification discussed in text, using MAR_{ar} and offsets between foraminifera and aragonite ages (overview of index markers in Table 3).

Castanier et al. [2000], and *Langdon et al.* [2000] that increased temperature and salinity decrease the ΣCO_2, which must be removed from the water column to induce calcium carbonate nucleation. On the basis of their study, *Morse and He* [1993] argued that an unrealistic high drop in ΣCO_2 would be necessary to increase the saturation state to allow inorganic precipitation of aragonite. They concluded that microbial activity alone would not be able to force such a drop. Nonetheless, for this area precipitation of aragonite occurs in expected equilibrium with respect to oxygen and carbon isotopes (*Shinn et al.* [1989] and our own data). Moreover, from their precipitation experiments, *von Knorre and Krumbein* [2000] concluded that an increase of carbonate alkalinity, provided as a by-product of microbial physiological processes, was sufficient to induce calcium carbonate precipitation.

[44] Elevated current strength and enhanced mixing will lead to a faster exchange of carbonate ions, so increasing the aragonite saturation state on the platform. Next to photosynthetic and microbial activity, an additional rise in temperature enhances the removal of CO_2 from the water column. This increases the saturation state with respect to aragonite, allowing direct inorganic aragonite precipitation from the water column, promoted by stirred-up bottom sediment due to physical processes. The close correlation of aragonite production with $\delta^{18}O$-derived temperatures of *G. sacculifer* (Figure 11) suggests a temperature dependence of aragonite precipitation, if the geochemical conditions (e.g., saturation state) are appropriate. Higher resolution sampling of sediment core MD992201 in the upper section, where temperature, salinity and geochemical measurements are available, may give a better and more detailed insight into aragonite precipitation patterns.

6. Conclusions

[45] High-resolution data sets of aragonite accumulation, age differences between planktonic foraminiferal ages and aragonite ages within the individual samples, and paleotemperatures derived from *G. sacculifer* from the Bahamian sediment core MD992201 (leeward margin of Great Bahama Bank) provide a detailed overview of the paleoclimatic and paleoceanographic conditions from 7230 years BP until the present time.

[46] Through MAR_{ar}, the age differences, and temperature distribution, relative aragonite production, changes and relative paleocurrent strengths have been deduced. Aragonite precipitation on GBB occurs in isotopic equilibrium and precipitation rates are dependent on geochemical parameters (particularly aragonite saturation state). The close correlation of fluctuations in aragonite precipitation with temperature-salinity conditions illustrates the effect of temperature on the CO_2 solubility in seawater. Additional CO_2 loss due to microbial activity and plankton blooms may enhance aragonite precipitation.

[47] Deduced relative paleocurrent strengths on GBB are in accordance with results from studies in the Gulf of Cadiz, investigating intensities of the Mediterranean Outflow Water [*Mulder et al.*, 2002; *Heilemann*, 2000; *Sierro et al.*, 1999]. Our results indicate high current velocities during 6000–5100 years BP, 3500–2700 years BP, and 1600–700 years BP, whereas the time intervals 5100–3500 years BP, 2700–1600 years BP, and 700–100 years BP are characterized by relatively slower current speeds.

[48] Variable current strength, geochemical parameters, and temperature-salinity conditions are functions of climatically driven changes in atmospheric and oceanic circulation. As water masses affecting GBB are derived from the North Atlantic Subtropical Gyre driven by the intensity and position of the North Atlantic westerlies and the northeasterly trade winds, the deduced current parameters give valuable information concerning the behavior of the North Atlantic atmospheric circulation through Mid- to Late Holocene times.

[49] The knowledge of the latitudinal position and strength of the NA atmospheric system (low- and high-pressure fields, ITCZ, trade wind belt, westerlies) is of major interest to reconstruct paleoclimatic conditions in the regions affected by the North Atlantic circulation (e.g., Caribbean, Africa, Europe and North America).

[50] Current strength and atmospheric conditions fluctuate in a millennial mode. Detailed time series analysis of the MD992201 data sets are in preparation (S. Roth and J. J. G. Reijmer, manuscript in preparation, 2003) and will provide information about North Atlantic climatic changes and behavior of the oceanic circulation on centennial to decadal timescales.

[51] The high potential of sediment cores from Holocene highstand wedges has largely been overlooked with respect to paleoclimatology and paleoceanography. Comparable cores from the Indian and Pacific oceans would provide data sets, which could explain the global atmospheric and oceanographic connections and help to improve global circulation models.

[52] **Acknowledgments.** We thank the captain and crew of the research vessel *Marion Dufresne* for technical assistance during the shipboard work. This study was supported by the German Science Foundation (Images Program to J.R. and DFG-RE 1051/9 to S.R. and J.R.). Special thanks to S. K. Boss, E. Rohling, and M. Tucker for reviewing and significantly improving this manuscript.

References

Agrawal, Y. C., I. N. McCave, and J. B. Riley (1991), Laser diffraction size analysis, in *Principles, Methods, and Application of Particle Size Analysis*, edited by J. P. M. Syvitski, pp. 119–128, Cambridge Univ. Press, New York.

Atkinson, L. P., T. Berger, P. Hamilton, E. Waddell, K. Leaman, and T. N. Lee (1995), Current meter observations in the Old Bahama Channel, *J. Geophys. Res.*, *100*(C5), 8555–8560, 1995.

Boardman, M. R., A. C. Neumann, P. A. Baker, L. A. Dulin, R. J. Kenter, G. E. Hunter, and K. B. Kiefer (1986), Banktop responses to Quaternary fluctuations in sea level recorded in periplatform sediments, *Geology*, *14*, 28–31.

Boss, S. K., and A. C. Neumann (1993), Physical versus chemical processes of "whiting" formation in the Bahamas, *Carbonates Evaporites*, *8*(2), 135–148.

Boss, S. K., and K. A. Rasmussen (1995), Misuse of Fischer plots as sea-level curves, *Geology*, *23*(3), 221–224.

Broecker, W. S., and T. Takahashi (1966), Calcium carbonate precipitation on the Bahama Banks, *J. Geophys. Res.*, *71*(6), 1575–1602.

Broecker, W. S., A. Sanyal, and T. Takahashi (2000), The origin of Bahamian whitings revisited, *Geophys. Res. Lett.*, *27*(22), 3759–3760.

Carew, J. L., and J. E. Mylroie (1997), Geology of the Bahamas, in *Geology and Hydrogeology of Carbonate Islands*, edited by H. L. Vacher and T. M. Quinn, pp. 91–139, Elsevier Sci., New York.

Carew, J. L., J. E. Mylroie, and S. J. Schwabe (1998), The geology of South Andros Island, Bahamas: A reconnaissance report, *Cave Karst Sci.*, *25*(2), 57–66.

Castanier, S., G. Metayer-Levrel, and J.-P. Perthuisot (2000), Bacterial roles in the precipitation of carbonate minerals, in *Microbial Sediments*, edited by R. E. Riding and S. M. Awramik, pp. 32–39, Springer-Verlag, New York.

Cloud, P. E. (1962b), Environment of calcium carbonate deposition west of Andros Island, Bahamas, *U.S. Geol. Surv. Prof. Pap.*, *350*, 1–138.

Demicco, R. V., and L. A. Hardie (2002), The "Carbonate Factory" revisited: A reexamination of sediment production functions used to model deposition on carbonate platforms, *J. Sediment. Res.*, *72*(6), 849–857.

Duan, Z., and R. Sun (2003), An improved model calculating CO_2 solubility in pure water and aqueous NaCl solutions from 273 to 533 K and from 0 to 2000 bar, *Chem. Geol.*, *193*, 257–271.

Ehrmann, W. U., and J. Thiede (1985), *History of Mesozoic and Cenozoic Sediment Fluxes to the North Atlantic Ocean*, 109 pp., Schweizerbart, Stuttgart.

Enos, P. (1974), Surface sediment facies of the Florida-Bahamas Plateau, *Map Ser. MC-5*, no. 4, Geol. Soc. of Am., Boulder, Colo.

Fairbanks, R. (1989), A 17,000 year glacio-eustatic sea level record: Influence of glacial melting rates on the Younger Dryas event and deep-ocean circulation, *Nature*, *342*, 637–642.

Ginsburg, R. N. (1956), Environmental relationships of grain size and constituent particles in some South Florida carbonate sediments, *Am. Assoc. Petrol. Geol. Bull.*, *40*(10), 2384–2427.

Heilemann, K. (2000), Hydrodynamische Änderungen des Mittelmeerausstromwassers und deren Abbildung in den Sedimenten des Iberischen Kontinentalhangs, Ph.D. thesis, Christian-Albrechts-Univ., Kiel.

Hernandez, J. L., D. Erickson III, and P. Ginoux (2001), Atmospheric iron flux and surface chlorophyll in the north-western tropical Atlantic, paper presented at IX COLACMAR Congress, Univ. Nac. De Colombia, San Andres.

Hine, A. C., and A. C. Neumann (1977), Shallow carbonate-bank-margin growth and structure, Little Bahama Bank, Bahamas, *Am. Assoc. Petrol. Geol. Bull.*, *61*, 376–406.

Hine, A. C., J. Wilber, J. M. Bane, A. C. Neumann, and K. R. Lorenson (1981a), Offbank transport of carbonate sands along open leeward bank margins: Northern Bahamas, *Mar. Geol.*, *42*, 327–348.

Hine, A. C., R. J. Wilber, and A. C. Neumann (1981b), Carbonate sand bodies along contrasting shallow bank margins facing open seaways in northern Bahamas, *Am. Assoc. Petrol. Geol. Bull.*, *65*, 261–290.

Langdon, C., T. Takahashi, C. Sweeney, D. Chipman, J. Goddard, F. Marubini, H. Aceves, H. Barnett, and M. J. Atkinson (2000), Effect of calcium carbonate saturation state on the calcification rate of an experimental coral reef, *Global Biogeochem. Cycles*, *14*, 639–654.

Leaman, K. D., P. S. Vertes, L. P. Atkinson, T. N. Lee, P. Hamilton, and E. Waddell (1995), Transport, potential vorticity, and current/temperature structure across northwest Providence and Santaren Channels and the Florida current off Cay Sal Bank, *J. Geophys. Res.*, *100*(C5), 8561–8569.

Lee, T. N., W. E. Johns, R. J. Zantopp, and E. R. Fillenbaum (1996), Moored observations of Western Boundary Current variability and thermohaline circulation at 26.5°N in the subtropical North Atlantic, *J. Phys. Oceanogr.*, *26*, 962–983.

Loizeau, J.-L., D. Arbouille, S. Santiago, and S.-P. Vernet (1994), Evaluation of a wide range laser diffraction grain size analyser for use with sediments, *Sedimentology*, *41*, 353–361.

Lowenstam, H. A., and S. Eppstein (1957), On the origin of sedimentary aragonite needles of the Great Bahama Bank, *J. Geol.*, *65*, 364–375.

MacIntyre, I. G., and R. P. Reid (1992), Comment on the origin of aragonite needle mud: A picture is worth a thousand words, *J. Sediment. Petrol.*, *62*(6), 1095–1097.

MacIntyre, I. G., and R. P. Reid (1995), Crystal alteration in a living calcareous alga (*Halimeda*): Implications for studies in skeletal diagenesis, *J. Sediment. Res.*, *A65*, 1143–1153.

McCave, I. N. (1972), Transport and escape of fine-grained sediment from shelf areas, in *Shelf Sediment Transport*, edited by D. J. P. Swift, D. B. Duane, and O. H. Pilkey, pp. 225–248, Van Nostrand Reinhold, New York.

Milliman, J. D. (1974), Carbonates and the ocean, in *Marine Carbonates (Pt 1)*, edited by J. D. Milliman, pp. 3–15, Springer-Press, New York.

Milliman, J. D., D. Freile, R. P. Steinen, and R. J. Wilber (1993), Great Bahama Bank aragonitic muds: Mostly inorganically precipitated, mostly exported, *J. Sediment. Petrol.*, *63*(4), 589–595.

Morse, J. W., and S. He (1993), Influences of T, S and P_{CO2} on the pseudo-homogeneous precipitation of $CaCO_3$ from seawater: Implications for whiting formation, *Mar. Chem.*, *41*, 291–297.

Morse, J. W., and F. T. Mackenzie (1990), in *Developments in Sedimentology*, 707 pp. Elsevier Sci., New York.

Morse, J. W., F. J. Millero, V. Thurmond, E. Brown, and H. G. Ostlund (1984), The carbonate chemistry of Grand Bahama Bank waters: After 38 years, another look, *J. Geophys. Res.*, *89*, 3604–3614.

Moulin, C., C. E. Lambert, F. Dulac, and U. Dayan (1997), Control of atmospheric export of dust from North Africa by the North Atlantic Oscillation, *Nature*, *387*, 691–694.

Mulder, T., et al. (2002), Past deep-ocean circulation and the paleoclimate record: Gulf of Cadiz, *Eos Trans. AGU*, *83*(43), 481, 487–488.

Murray, R. W., and M. Leinen (1996), Scavenged excess Al and its relationship to bulk Ti in biogenic sediment from the central equatorial Pacific Ocean, *Geochim. Cosmochim. Acta*, *60*, 3869–3878.

Neumann, A. C., and L. S. Land (1975), Lime mud deposition and calcareous algae in the Bight of Abaco, Bahamas: A budget, *J. Sediment. Petrol.*, *45*(4), 763–786.

Newell, N. D., and J. K. Rigby (1957), Geological studies on the Great Bahama Bank, in *Regional Aspects of Carbonate Deposition*, edited by R. J. LeBlanc and J. G. Breeding, pp. 15–79, Soc. for Sediment. Geol., Tulsa, Okla.

Nyberg, J., B. A. Malmgren, A. Kuijpers, and A. Winter (2002), A centennial-scale variability of tropical North Atlantic surface hydrography during the late Holocene, *Palaeogeogr. Palaeoclimatol. Palaeoecol.*, *183*, 25–41.

Purdy, E. G. (1963a), Recent calcium carbonate facies of the Great Bahama Bank. 1. Petrography and reaction groups, *J. Geol.*, *71*(3), 334–355.

Purdy, E. G. (1963b), Recent calcium carbonate facies of the Great Bahama Bank. 2. Sedimentary facies, *J. Geol.*, *71*(3), 472–497.

Robbins, L. L., and P. L. Blackwelder (1992), Biochemical and ultrastructural evidence for the origin of whitings: A biologically induced calcium carbonate precipitation mechanism, *Geology*, *20*, 464–468.

Robbins, L. L., Y. Tao, and C. A. Evans (1997), Temporal and spatial distribution of whitings on Great Bahama Bank and a new lime mud budget, *Geology*, *25*(10), 947–950.

Sarnthein, M., G. Tetzlaff, B. Koopmann, K. Wolter, and U. Pflaumann (1981), Glacial and interglacial wind regimes over the eastern subtropical Atlantic and north-west Africa, *Nature*, *293*, 193–196.

Shinn, E. A., R. P. Steinen, B. H. Lidz, and P. K. Swart (1989), Whitings, a sedimentological dilemma, *J. Sediment. Petrol.*, *59*(1), 147–161.

Sierro, F. J., J. A. Flores, and J. Baraza (1999), Late glacial to recent paleoenvironmental changes in the Gulf of Cadiz and formation of sandy contourite layers, *Mar. Geol.*, *155*(1–2), 157–172.

Singer, J. K., J. B. Anderson, M. T. Ledbetter, I. N. McCave, K. P. N. Jones, and R. Wright (1988), An assessment of analytical techniques for the size analysis of fine-grained sediments, *J. Sediment. Petrol.*, *58*, 534–543.

Smith, C. L. (1940), The Great Bahama Bank, *J. Mar. Res.*, *3*, 147–189.

Smith, N. P. (1995), On long-term net flow over Great Bahama Bank, *J. Phys. Oceanogr.*, *25*, 679–684.

Stuiver, M., and H. A. Polach (1977), Discussion: Reporting of ^{14}C Data, *Radiocarbon*, *19*(3), 355–363.

Stuiver, M., P. J. Reimer, E. Bard, J. W. Beck, G. S. Burr, K. A. Hughen, B. Kromer, F. G. McCormac, J. van der Plicht, and M. Spurk (1998), INTCAL98 Radiocarbon age calibration, 24,000-0 cal BP, *Radiocarbon*, *40(3)* (1), 12–14.

Taylor, S. R., and S. M. McLennan (1985), *The Continental Crust: Its Composition and Evolution*, 312 pp., Blackwell Sci., Malden, Mass.

Thompson, J. B., S. Schultze-Lam, T. J. Beveridge, and D. J. Des Marais (1997), Whiting events: Biogenic origin due to the photosynthetic activity of cyanobacterial picoplankton, *Am. Soc. Limnol. Oceanogr.*, *42*(1), 133–141.

von Knorre, H., and W. E. Krumbein (2000), Bacterial calcification, in *Microbial Sediments*, edited by R. E. Riding and S. M. Awramik, pp. 25–31, Springer-Verlag, New York.

Wachter, E., and J. M. Hayes (1985), Exchange of oxygen isotopes in carbon-dioxide—Phosphoric acid systems, *Chem. Geol.*, *52*, 365–374.

Wajsowicz, R. C. (2002), A modified Sverdrup model of the Atlantic and Caribbean circulation, *J. Phys. Oceanogr.*, *32*, 973–993.

Wilber, R. J., J. D. Milliman, and R. B. Halley (1990), Accumulation of bank-top sediment on the western slope of Great Bahama Bank: Rapid progradation of a carbonate megabank, *Geology*, *18*, 970–974.

Wilber, R. J., J. Whitehead, R. B. Halley, and J. D. Milliman (1993), Carbonate periplatform sedimentation by density flows: A mechanism for rapid off-bank and vertical transport of shallow-water fines: Comment and reply, *Geology*, *21*, 667–669.

Wilson, P. A., and H. H. Roberts (1992), Carbonate periplatform sedimentation by density flows: A mechanism for rapid off-bank and vertical transport of shallow-water fines, *Geology*, *20*, 713–716.

Wilson, P. A., and H. H. Roberts (1995), Density cascading: Off-shelf sediment transport, evidence and implications, Bahama Banks, *J. Sediment. Res.*, *A65*, 45–56.

J. J. G. Reijmer and S. Roth, Wischhofstr. 1–3, D-24148 Kiel, Germany. (jreijmer@geomar.de; sroth@geomar.de)